Title- Age associated alterations in the cortical representation of cardiac signals: A heartfelt tale

Authors - Kirti Saluja[1], Dipanjan Roy[2], Arpan Banerjee[1]*

Affiliations –

[1]National Brain Research Centre, NH-8, Manesar, Haryana – 122052

[2] Centre for Brain Science and Applications (CBSA), School of AIDE, Indian Institute of Technology, Jodhpur - 342030

* Corresponding Author

Email : arpan@nbrc.ac.in

Keywords: ECG, MEG, heart, brain-body, HERs, evoked

Abstract

Neural representation of cardiac rhythms, known as heartbeat evoked responses (HERs), provide a avenue for investigating the interaction between the brain and the heart, pivotal for various physiological and cognitive functions. Concomitantly, age is recognized as a significant factor influencing this interaction, given its impact on both the structural and functional aspects of the brain and the cardiovascular system. Nonetheless, the precise nature of this interaction during the healthy ageing process remains elusive. This study aims to investigate how the influence of cardiac rhythms on spontaneous brain activity varies with age, using HERs as a measure. Subsequently, it aims to explore the mechanism underlying HERs generation and characterize the brain networks that prominently represent HERs from a large (N = 620) human healthy ageing dataset (18-88 years). The results show that HERs exhibit time-locked activity around 180-320 ms post R-peak of the electrocardiogram (ECG) waveform, with significant decrease in HER amplitude across age for both the genders. Furthermore, inter-trial phase coherence (ITPC) analysis indicates that cardiac signals modulate the phases of the ongoing neural oscillations rather than altering the spectral power. Causal functional maps among brain areas computed using Granger causality (GC) reveals consistent connectivity in the fronto-temporal network, though with varying strength across age groups revealing a compensatory mechanism in play to maintain homeostasis. Overall, these findings provide a comprehensive understanding of the interaction between heart and brain in healthy ageing and present opportunities to identify non-invasive markers for characterizing pathological development in neurological and cardiovascular functions.

1. Introduction

The brain serves a twofold role - maintaining internal stability through homeostasis and enabling cognitive processes essential for our day-to-day functioning and interaction with the environment. While extensive research has explored how the brain process the signals emerging from the external environment (e.g., auditory, visual) and how this processing affected by age (de Dieuleveult et al., 2017; Jayakody et al., 2018; Rauschecker & Tian, 2000). However, understanding the effects of age on the processing of the signals emerging from the internal environment (e.g., signals from visceral organs such as the heart) referred to as interoception (Craig, 2002; Critchley et al., 2004), still presents a challenge (Azzalini et al., 2019; Murphy et al., 2018). This question will have tremendous translational significance, since there have been reports of declining cardiovascular health predominantly impacting the older population as they age (Khalsa et al., 2009; North & Sinclair, 2012) concomitantly with a significant increase in life expectancy leading to an rise in the population of older individuals according to the World Health Organisation (WHO) (Padeiro et al., 2023).

The heart is physically connected with the nervous system and needs to generate rhythmic pumping of oxygenated blood into the body and deoxygenated blood into the lungs (Shen & Zipes, 2014). The signaling between the heart and the brain is essentially a two-way communication (Chen et al., 2017), failure of which can result in cardiac arrhythmia (Saunders & Jenkins, 1973) and stroke (Kallmünzer et al., 2012). Cardiac signals reach the brainstem and thalamus via the dorsal root ganglion and vagus nerve, proceeding to the hypothalamus, amygdala, anterior cingulate cortex and insula and finally extending to the ventral medial prefrontal cortex and orbitofrontal cortex (Thayer & Lane, 2009). The information from these cardiac signals is relayed, serving as ‘internal stimuli’ to the brain along with the external stimuli (continuous or discrete), and is recognized for its role in modulating the dynamics and function of the brain such as arousal (Luft & Bhattacharya, 2015), predictive coding (Park et al., 2014), interoceptive accuracy (Garfinkel et al., 2015; Pollatos & Schandry, 2004), heart diseases (Khalsa & Verdonk, 2022), somatosensory perception (Al et al., 2020), attention (Petzschner et al., 2019), consciousness (Babo-Rebelo et al., 2016), ageing (Kamp et al., 2021) and mental disorders (Schulz et al., 2015; Terhaar et al., 2012).

Heartbeat evoked responses (HERs) are the neural responses time locked to key events in electrocardiogram (ECG) waves (usually the R and/or T peak) obtained by using either invasive techniques such as intracranial encephalography (iEEG) and stereo-encephalography (sEEG) or non-invasive neuroimaging techniques such as magnetoencephalography (MEG) and electroencephalography (EEG) (Montoya et al., 1993). HERs can be a candidate signal for investigating the representation of cardiac dynamics in cortical structures since ECG captures the physiological heart function and is a widespread measure of cardiac health. The existing literature reports about the predictive nature of HERs, for instance, Banellis and Cruse (Banellis & Cruse, 2020) showed how the brain uses temporal cues from cardiac signals to predict auditory stimuli using HERs. Furthermore, Al and colleagues (Al et al., 2020) showed the conscious perception and somatosensory evoked potential are shaped by the timing at which the somatosensory stimulus is presented with reference to the cardiac cycle, along with the pre-stimulus HERs. While the investigation on HERs during resting state remains limited, one study (Kim & Jeong, 2019) proposed that the heartbeat induces phase synchronization in the cortical regions within the theta frequency band during rest, forming a network known as the heartbeat-induced network (HIN). The left inferior temporal gyrus and para hippocampal gyrus are identified as hub regions within this network, which further affects emotion regulation. Furthermore, (Kamp et al., 2021) recently examined age-associated alterations in the cortical representation of cardiac rhythms using HERs. Their study highlights increased HERs amplitude in older adults and establishes a correlation between HER amplitude and scores from metacognitive judgement task. This investigation is pertinent given that ageing affects both the structural and functional aspects of the brain (Climie et al., 2023; North & Sinclair, 2012; Sahoo et al., 2020; Thuwal et al., 2021). However, the study is constrained by certain limitations, including a restricted dataset and a lack of comprehensive exploration of the age-related mechanisms and connectivity associated with the cortical representation of cardiac signals.

Therefore, the primary objective of this research is to delve into the impact of age on the cortical representation of the cardiac signals and the alterations in the connectivity patterns between the heart and the brain in the resting state. In this work, we achieve this by applying signal processing tools on HERs to uncover the potential underlying mechanisms and cortical network involved in its generation, using a comprehensive dataset of healthy ageing individuals aged 18-88 years, with a large-sample size (N = 620). The process of healthy ageing encompasses complex structural and functional changes in the brain and body, occurring at molecular, cellular and vascular levels. In particular, there is a reduction in the brain volume (Peters, 2006), degradation of prefrontal cortex (Kang et al., 2022)., among other factors, along with vascular ageing which is characterized by gradual deterioration of arterial structure and function across age (Climie et al., 2023). Additionally, advancing age is associated with an increased risk of stroke due to deteriorating cardiovascular health, cerebral modification and leading to subsequent impaired cognition (Khalsa et al., 2009; Khalsa & Verdonk, 2022; Krishnamoorthy et al., 2016; Peters, 2006). Given these fundamental pieces of evidence, we hypothesize that the representation of the cardiac information varies across healthy ageing, as reflected in the pattern of HERs and dynamical properties of its underlying brain network. Furthermore, investigating whether there are any compensatory mechanisms involved in this regard could aid in developing effective functional interventions in the prevention of stroke and cardiovascular risks among the elderly population. With the motivations outlined above, this document is structured as follows: (1) investigating the trend of HERs as function of lifespan ageing and to establish it as a viable tool for assessing healthy homeostasis (2) an examination of the phase resetting versus amplitude driven mechanisms behind the generation of HERs using wavelet transformation and (3) an analysis of the neural network associated with HERs, including its connection to the heart using statistical measure to estimate causal maps in neural circuit, viz, Granger causality (Barnett & Seth, 2014; Dhamala et al., 2008; Kamiński et al., 2001).

2. Results

2.1. Physiological metrics of cardiovascular health across lifespan ageing

We followed the pipeline presented in **Figure 1** to analyze the electrocardiographic (ECG) and magnetoencephalographic (MEG) data from the Cam-CAN cohort (Shaftoo et al 2014), comprising 620 participants aged 18 to 88 years. To assess the cardiovascular health, we utilized electrocardiographic parameters including inter-beat interval (IBI), heart rate variability (HRV), heart rate (HR) and blood pressure (BP) indicators such as systolic and diastolic pressure (**Figure 2.A**). These parameters were derived from ECG time series and blood pressure scores provided by Cam-CAN. We observed that IBI significantly decreases (r = -0.0994, p = 0.0133; **Figure 2.B**) and HR significantly increases across age (r = 0.1121; p = 0.0052**; Figure 2.D**) at 95% confidence levels. However, HRV does not decrease significantly across age (r= -0.0022, p= 0.9573; **Figure 2.C**). In case of the trend of blood pressure scores across age, systolic pressure was significantly increasing (r = 0.4370, p<0.001; **Figure 2.E**) whereas diastolic pressure remained unchanged across age (r = 0.0734; p: 0.0910; **Figure 2.F**). Refer to the **supplementary table 1** for additional details regarding the model.

2.2 Heartbeat evoked responses (HERs) across lifespan

Figure 3.B shows the global HERs calculated for three age groups i.e., young (18-40 years), middle (41-60 years), and old (61-87 years). We found a main effect of age on HERs (F(2,619) = 9.47, p = 0.0001) while the effect of gender became non-significant (F(1,619) = 0, p = 0.9631) in the early phase (180-320 ms post R peak) window. Furthermore, an interaction of both factors were found to be non-significant (F(2,619) = 0.33, p = 0.7213). Refer to Supplementary Table 3 for further details. To validate this result, we calculated the HERs with respect to the shuffled ECG time series mentioned in section 4.7, no time locked activity was observed concerning the non-R time points. Further, linear regression analysis shows that the HERs amplitude extracted from the window of 180-320 ms post R peak of the ECG waveform significantly decreases across age ($r= -0.1963$; $p<0.001$) (**Figure 3.D**). Refer to Supplementary Table 4 for specifications of the regression model.

2.3. Relationship of cardiac rhythms and ongoing neural oscillations

We investigated to substantiate the hypothesis that cardiac rhythms induce patterned changes in neural oscillations via phase resetting rather than a mere additive enhancement in spectral power (Park et al., 2018). The measure of inter-trial phase coherence (ITPC, see methods section for details) was used to test this idea, which increases if phase resetting occurs. Our findings indicate a significant increase in ITPC during the time interval of 180-320 ms following the R peak across all age groups (**Figure 4.A**: critical value of ITPC; $p < 0.05$). However, no time locked activity was observed when we examined ITPC relative to the shuffled ECG time series (preserving the physiological IBI) (**Figure 4.B**). Furthermore, it was observed that predominant resetting of phase occurred within theta frequency band among young and middle age-group participants. However, the older age group, notable activity was observed in the alpha frequency band in addition to the activity in the theta band. The power analysis in the time-frequency domain showed no significant enhanced synchronization time locked to the R peaks (**Figure 4.C**) either for shuffled R peaks (**Figure 4.D**) of the ECG waveform (two-tailed cluster permutation test at $p = 0.05$). Interestingly, a significant increase in the ITPC values was observed across age in the theta frequency band ($r= 0.2236$; $p<0.001$) (**Figure 4.E**). No significant correlation was observed between mean ITPC values and mean power extracted at around 180-320 ms post R peak of the ECG waveform ($r = 0.0596$; $p = 0.1382$) from each participant (**Figure 4.F**).

2.4. Underlying cortical sources of HERs

We employed eLORETA (as detailed in section 2.9) to estimate the underlying sources contributing to HERs observed at the sensor level within the 180-320 ms window post R peak of the ECG time series. After the source power was computed for each participant, a grand averaging of the source power was calculated across all the 620 participants whose brain volumes were normalized to a common template (Colin 27) and subjected to statistical significance testing. Source power surpassing the 95th percentile threshold was considered as significant sources of the HERs in the resting state condition. Furthermore, three significant clusters were obtained using k-means clustering and centroid of each cluster was considered the significant source whose nearest MNI coordinate was identified. The cortical sources of HERs (along with their nearest MNI coordinates) were found to be: Right Orbitofrontal Cortex (MNI coordinates = 7, 26, -20), Right Anterior Prefrontal Cortex (8,50,2) and Left Temporal Pole (-47, 10, -17). These significant sources were visualized using the *'ft_sourceplot'* function within Fieldtrip (**Figure 5**).

2.5. Directed functional connectivity among cortico-cortical nodes

With the motivation to investigate the directional interaction among the cortical sources involved in the processing of cardiac information, as well as the directional interplay between the cortical sources of HERs and ECG time series, we conducted Granger Causality (Barnett & Seth, 2014; Dhamala et al., 2008; Geweke, 1982) analysis (**Refer to section 2.11**). We observed interactions among various brain sources and between brain sources and cardiac time series across different age groups and varying strengths of GC (**Supplementary Table 7**). The significant unidirectional flows between the brain sources are represented with → and bi-directional flow as ⟷ in the text. In all the age groups, we observed R OFC ⟷ R Ant.

PFC, R OFC ←→ L Temp Pole and R Ant. PFC → L Temp Pole. All the causations were statistically significant and are illustrated in **Figures 6.b. and Table 2**.

Table 2: Pairwise casual influence among the cortical sources of HERs with their averaged causal strength. All the causal connections shown are significant.

From	**To**	**Young**	**Middle**	**Old**
R Orbitofrontal Cortex	R Anterior Prefrontal Cortex	0.1558	0.1537	0.1487
R Anterior Prefrontal Cortex	R Orbitofrontal Cortex	0.2226	0.2412	0.2324
R Orbitofrontal Cortex	L Temporal Pole	0.1424	0.1496	0.1491
L Temporal Pole	R Orbitofrontal Cortex	0.2590	0.2951	0.2897
R Anterior Prefrontal Cortex	L Temporal Pole	0.2103	0.2424	0.2332

For continuous analysis, we found that the casual information flow (GC values) from the Left Temporal Pole to Right Orbitofrontal cortex ($r = 0.1728$; $p < 0.001$) and from the Right Anterior Prefrontal cortex to Left Temporal pole ($r = 0.1530$; $p < 0.001$) GC values significantly increase across age.

3. Discussion

Our study attempted to investigate the age associated changes in the cortical representation of the cardiac rhythms, generation of HERs and underlying neural networks. We have identified four key empirical observations from our study. *First,* we observed a time locked activity in 180-320 ms post R peak of the ECG waveform termed as HERs at the sensor level (**Figure 3**) which is validated over a large number of samples (N = 620). This pattern of HERs amplitude decreases across age, suggesting an age-related alteration in the processing of cardiac rhythm. *Second*, the underlying process leading to the generation of HERs suggest a phase resetting of the spontaneous brain oscillations at the 180-320 ms post R peak of the ECG waveform rather than additive spectral power enhancement in theta band (4-8 Hz) frequency band at the sensor level (**Figure 4**). We observed a linear increasing trend of the ITPC values across age in the theta (4-8 Hz) frequency band, implying a varying impact of age on the synchronization of cortical regions induced by cardiac rhythms. *Third*, we found the neural sources of HERs during the resting state, primarily located in the right orbitofrontal cortex, right anterior prefrontal cortex and left temporal pole (**Figure 5**). *Fourth*, the directed flow between the neural sources to be R OFC ←→ R Ant. PFC, R OFC ←→ L Temp Pole and R Ant. PFC → L Temp Pole (**Figure 6**). The GC values obtained for these casual connections were observed to show a pattern across age although the nature of casual directions never changed. The trend of information transfer from the left temporal pole to the right orbitofrontal cortex and the right anterior prefrontal cortex to the left temporal pole observed to be linearly increasing across age, suggesting both top-down and bottom-up functional processing increases in fronto-temporal circuits might be as a compensatory mechanism. Such shifting of cognition architecture was proposed by earlier studies (Spreng & Turner, 2019). Based on our findings, we have identified age associated alterations in the cortical representation of cardiac rhythms, as estimated by HERs, which can be one missing dominant player in cognition network shifts and which, to be the best of our knowledge, have not been previously reported. In the subsections, we delve into the implications of salient findings from our study.

Functional relevance of age-related changes in HERs at resting state

HERs are the neural responses to the cardiac rhythms, believed to convey cardiac information to central autonomic regions and proposed as an indicator of internal body awareness known as interoception (Banellis & Cruse, 2020; Pollatos & Schandry, 2004). HERs exhibit modulations influenced by various factors, including cardiac condition (Kumral et al., 2022), attention (Petzschner et al., 2019), interoceptive awareness (Khalsa et al., 2009), and age (Kamp et al., 2021), to mention a few. What significance do HERs hold during the resting state, and why do they undergo age-related changes? To address this knowledge gap, our study represents the first attempt to examine the modulation of HERs during the resting state using a large lifespan dataset. One of the significant findings from our study is the presence of time locked neural activity at 180-320ms post R peak of the ECG waveform, and we observed a notable decrease in HERs amplitude across age at the resting state. Furthermore, HERs was calculated for different genders (male and female). We found that HERs significantly decreases across age for both the gender groups. The baroreceptors present in the myocardium are known to transmit information regarding the mechanical variability and pressure differences in the cardiac muscles which are reflected at the cortical level (Gray et al., 2007). The time-locked activity observed in our study, occurring approximately 180-320ms post R peak of the ECG waveform, corresponds to the time when the heartbeat signals enter the CNS (Eckberg & Sleight, 1992). Moreover, the amplitude of the HERs is linked to heartbeat perception (Pollatos & Schandry, 2004); hence we speculate that lower HERs amplitude observed in the older adults suggest a decrease in interoceptive awareness (Khalsa et al., 2009). However, it is important to note a limitation of our study: we did not have an interoceptive awareness score, which prevented us from correlating the HERs amplitude with interoceptive scores to comment on this aspect directly. Also, the changes in the patterns of HERs amplitude across age observed at the cortical level can be associated with the structural change brain undergoes such as atrophy in the white matter (Pathak et al., 2022), degradation of the prefrontal cortex (Cabeza & Dennis, 2013; Zanto & Gazzaley, 2019) and many more. Nonetheless, the observation of HERs amplitude decrease offers a window to test many of these mechanisms in the future.

Phase resetting as the foundation of HERs generation

The present findings could give us a possible basis for generating HERs, the heartbeat acts like an "internal trigger" to the neural oscillations and works by resetting the phase of the spontaneous brain rhythms, rather than by additive evoked responses, as suggested (Park et al., 2018). They showed this observation in epileptic patients, further linking it to bodily self-consciousness. In our study, we observed ITPC around 180 ms post R peak of the ECG waveform with no change in the spectral power. On shuffling the R peaks of ECG waveform, no time locked activity was observed. Specifically, in the ITPC results, we observed activity primarily in the theta frequency band for the young and the middle age group whereas older participants, in addition activity in theta frequency band, alpha was also evident. Moreover, upon extracting ITPC values participant-wise within the theta band, we observed an increasing trend of ITPC across age. (Kim & Jeong, 2019) also reports that heartbeat induces cortical networks that synchronize in the theta band during resting state which could be relevant for understanding embodied cognition and emotions. Previous studies have shown that approximately 180 ms post R peak onset is when individuals process their heartbeat (Park et al., 2018) and this heartbeat perception can be affected by age (Khalsa et al., 2009). Ageing is associated not only with vascular stiffening throughout the body and the brain (Gauthier et al., 2013) but also with the changes in the spatiotemporal properties of the neural oscillations even at resting state (Sahoo et al., 2020; Thuwal et al., 2021). These changes have the potential to affect the neurovascular coupling and may contribute to the observed variations in ITPC across age. On the other hand, these results lay a groundwork for understanding how sensory stimulus is influenced by visceral states. For instance (Garfinkel et al., 2014) showed fear processing is enhanced when stimulus timing was matched with cardiac cycle e.g., when presented at systole the fear intensity increases as compared to diastole. Thus an immediate explanation for such findings may reside with the time-locked ITPC enhancement of brain rhythms of resting state with cardiac cycle.

Directed functional connectivity among the HERs sources

The cardiac signals are known to be relayed from brainstem all the way to cortical regions such as orbitofrontal cortex, insula, prefrontal cortex according to the neurovisceral theory (Thayer & Lane, 2000, 2009). In our study, we identified a network responsible for processing of cardiac signal during resting state, with hubs located in the orbitofrontal cortex, right anterior prefrontal cortex and left temporal pole. Kim and Jong (Kim & Jeong, 2019) found that heartbeat induces synchronization between different cortical areas such as parahippocampal gyrus and inferior temporal gyrus furthermore forms a heartbeat induced network (HIN). Additionally, they studied HIN with connection with the abnormal interoceptive processing in the mood disorder patients. Interestingly, in our study we observed existence of a bidirectional interaction between right orbitofrontal cortex and anterior frontal cortex, right orbitofrontal cortex and left temporal pole and unidirectional interaction between anterior prefrontal cortex to left temporal pole. The GC values obtained for these casual connection were observed to show a pattern across age although the nature of casual directions never changed. The trend of information transfer from left temporal pole to right orbitofrontal cortex and right anterior prefrontal cortex to left temporal pole observed to be linearly increasing across age suggesting both top-down and bottom-up functional processing increases in fronto-temporal circuits might be a compensatory mechanism to preserve the processing of the cardiac information across age. In line to our finding, recently (Pathak et al., 2022) utilized an in-silico whole brain model to demonstrate that enhancing the inter-areal coupling (global synaptic scaling) can mitigate the effects of increased axonal transmission delays caused by age-related white matter degradation. These findings highlight functional integration through neural synchrony as a crucial neuro-compensatory mechanism. This opens the avenue to investigate this network further as it as it is known that there are prominent age-related changes in the prefrontal cortex which might causing changes in the processing of the cardiac signals across age (Cabeza & Dennis, 2013; Zanto & Gazzaley, 2019).

In conclusion, healthy age induces alterations in the processing of cardiac signals, as demonstrated by HERs along with modulating the properties of spontaneous brain rhythms and as well as mechanistic operational principles of underlying networks. These findings offer valuable insights into comprehending the heart-brain interactions in the neurological disorders, cardiovascular conditions, or more broadly, how this interaction influences perception of the external world.

4. Methods

4.1. Dataset and Participants

The Cambridge Ageing Neuroscience cohort (Cam-CAN) is a large-scale, multimodal, cross-sectional, population based lifespan (18-88 years) study (Shafto et al., 2014; Taylor et al., 2017). The Cam-CAN project involved two stages. During the first stage, cognitive assessments and tests for hearing, vision, balance, and speeded response, were conducted on 2681 participants at their homes. The data collected during stage 1 was also used to screen participants for stage 2. Those with poor hearing, poor vision, neurologic diseases (such as stroke or epilepsy), or a score of less than 25 in the MMSE cognitive assessment examination were excluded from further participation. This study was conducted in accordance with the Helsinki Declaration, and received approval from local ethics committee, Cambridgeshire 2 Research Ethics Committee (reference: 10/H0308/50).

In the second stage of the project, 700 participants (50 men and 50 women from each age band) were screened and recruited to undergo testing at the Medical Research Council (United Kingdom) Cognition and Brain Sciences Unit (MRC-CBSU) in Cambridge. Participants underwent MRI scans, MEG recordings, and completed various psychological tests and neuroimaging assessments during this stage. In the current investigation, we have included resting-state MEG data for analysis, which was acquired concurrently with ECG recordings. Moreover, given that the primary objective of the present study is to examine the cortical representation of the heartbeat across different age groups, the participants were subjected to a thorough screening process for cardiovascular disorders and associates disorders. Those who had history of the uncontrolled high blood pressure, stroke or undergone any heart operation or used any blood vessel device/pacemaker were subsequently excluded from the study cohort.

In the present investigation, we employed continuous and categorical approaches to comprehensively capture various aspects of age-related functional differences. For the continuous analysis, we treated each participant's age as a single data point. Conversely, for the categorical analysis, we segregated the participants into three distinct groups based on their age. Young adults (18-40 years), Middle adults (41-60 years) and Older adults (61-87 years) as outlined in **Table 1**.

Table 1: Demographic information of Cam-CAN Neuroimaging cohort

Measure	Young Adults	Middle Adults	Older Adults
N	177	198	245
Age range (years)	18-40	41-60	61-87
Mean age ± std (years)	31.32 ± 6.04	50.28 ± 5.64	72.88 ± 7.27
Female %	48.02	51.01	48.39

4.2. Data Acquisition

MEG Resting State

The MEG data utilized in this study were obtained from the publicly available Cam-CAN repository, accessible at http://www.mrc-cbu.cam.ac.uk/datasets/camcan/. For all the participants, MEG data were acquired by Elekta Neuromag, Helsinki, using a total of 306 channels, including 102 magnetometers and 204 orthogonal planar gradiometers. The data was collected in a magnetically shielded room (MSR) with low lighting. Data sampling was performed at 1000 Hz with a high-pass filter of 0.03 Hz. Head-position indicator (HPI) coils were used to continuously monitor the position of the participant's head within the MEG helmet. Additional electrodes were used to record horizontal and vertical electrooculogram (EOG) signals to monitor eye blinks and movements. The acquisition of eyes-closed resting-state MEG data was carried out for at least 8 minutes and 40 seconds.

ECG Resting State

ECG data were recorded concurrently with MEG acquisition using a pair of bipolar electrodes with a sampling rate of 1000 Hz. The acquisition lasted at least 8 minutes and 40 seconds.

4.3. Data Preprocessing

The Cam-CAN provided the MEG processed data, which underwent a pre-processing pipeline that involved temporal signal space separation to eliminate noise from HPI coils, environmental sources and continuous head motion correction. A max filter was used to remove the main frequency noise (50-Hz notch filter) and reconstruct any noisy channel. Further information on data acquisition and preprocessing can be found at (Cam-CAN et al., 2014; Taylor et al., 2017). We detrended the MEG time series, and a bandpass filter was applied with a 1-45 Hz range.

Further, we employed ICA (Independent Component Analysis) in MNE-Python to eliminate artifacts such as eye blink and cardiac field.

The ECG time series was detrended before passing it through the Pan-Tompkins algorithm (described in 2.3.1 section) to locate R-peaks in the ECG waveform. Participants were further screened on the basis of their quality of ECG signal (**Supplementary Table 1**). ECG signals were used to calculate parameters like variability of R-R interval, relative power of the QRS complex, skewness and kurtosis (**Supplementary Figure 1**). Following the screening, we performed our analysis pipeline on 620 participants.

4.4. Data Analysis

All the data analysis was conducted in MATLAB using custom-made scripts. First, the fieldtrip toolbox (https://www.fieldtriptoolbox.org/) was used to load the data in the '.fif' format (Oostenveld et al., 2010). The time series corresponds to the 309 x T where 309 are the total number of channels consisting of 102 magnetometers, 204 gradiometers, EOG, ECG and other auxiliary electrodes. For our analysis, we utilized 102 magnetometers from the MEG setup and a bipolar ECG electrode. The analysis pipeline is provided in **Figure 1**.

4.5. Pan-Tompkins Algorithm

The cardiac cycle consists of distinct peaks of P wave, QRS complex and T wave representing mechanical events in the cardiac muscles such as atrial contraction, ventricular contraction and ventricular relaxation respectively. We employed Pan-Tompkins algorithm to locate the QRS complex, the most prominent peak in the ECG waveform (Sedghamiz, 2014). The vector representing the time points of the ECG waveform was passed into the algorithm which involves several steps including bandpass filtering the ECG time series generally in the range of 5-15 Hz, squaring the time series, applying a derivative filter and finally identifying the location of QRS complex using the moving window approach. The algorithm can be found at (https://in.mathworks.com/matlabcentral/fileexchange/45840-complete-pan-tompkins-implementation-ecg-qrs-detector).

4.6. Cardiovascular Scores

The inter-beat interval (IBI) and heart rate variability (HRV) were determined by analyzing ECG signals. The R peaks, identified using the Pan-Tompkins algorithm (refer to section 2.5), were used to extract the IBI, representing the time difference between consecutive R peaks. The average IBI obtained was further used to calculate the heart rate (HR) - the number of heartbeats per unit time (beats/min). HRV was computed by calculating the standard deviation of the IBI, which represents the fluctuations in the time interval between consecutive heartbeats. IBI, HRV and HR were computed for each participant for an initial 60-seconds ECG recording (a short sampling window approach) (Lehavi et al., 2019). For each participant, cam-CAN recorded average systolic and diastolic pressure (recorded three times). To investigate the relationship between these cardiovascular scores and age, linear regression analysis was performed.

4.7. Heartbeat Evoked Responses (HERs)

To map the brain response time-locked to QRS peaks of ECG, the QRS peaks obtained from the Pan-Tompkins algorithm, were used as a trigger points to epoch the MEG time series. This allowed us to test the key hypothesis of whether interoceptive signals acts as the stimulant to the ongoing brain dynamics. Based on visual inspection, we could identify that a pre-stimulus of 200ms (prior to QRS peak) and a post-stimulus of 800ms (post to QRS peak) capture uniquely one complete cardiac cycle. HERs were computed using averaging across trials and channels.

For continuous analysis, the aforementioned HERs was averaged across the number of channels and epochs resulting in a 1 x 1000 dimensional vector where 1000 represents the time points. The amplitude values between 180-320 ms post R peak were extracted per subject. To normalize the data, we performed peak-to-peak subtraction by subtracting the maximum amplitude value from each amplitude value for each participant. For categorical analysis, the matrix was stacked according to the age group i.e., younger adults, middle adults, and older adults. The global HERs were obtained by averaging the matrix across channels and trials.

We performed a surrogate analysis to validate the presence of HERs obtained from time locking to R peak of the ECG waveform. This involved computing a shuffled HERs subject wise by randomly selecting non-R peaks to time lock essentially, random points from ECG time series excluding the R peaks, while maintaining the physiological IBI.

4.8. Assessment of the mechanism underlying HERs

4.8.1. Inter-trial phase coherence (ITPC)

ITPC analysis (Oostenveld et al., 2010) was performed on both the HERs time series synchronized with the R peak and the shuffled HERs time series time-locked to random points in ECG. We calculated power and phases using wavelet transformation in the frequency range of 4 to 20 Hz for all 102 magnetometers. We implemented the above method using *ft_freqanalysis* in MATLAB (Oostenveld et al., 2010). The ITPC values are computed using:

$$ITPC_f = [\frac{1}{n}\sum_{r=1}^{n} e^{i\theta}] \qquad (1)$$

wherein f derived is the frequency range at which the ITPC was calculated, $\frac{1}{n}\sum_{r=1}^{n}(\square)$ represents an average of complex vector over n trials; $e^{i\theta}$ is the Euler's formula where θ is phase angle derived from complex Fourier coefficients. The value of ITPC ranges between 0 and 1, with higher values of ITPC corresponding to higher phase consistency across trials. As ITPC values exhibit significant variations based on the number of trials or participants, for group analysis consistency, we randomly selected 177 participants (N of the lowly populated group, Table 1) within each group (Van Diepen & Mazaheri, 2018). To evaluate the significance of phase clustering, the ITPC values obtained were contrasted with a critical value, computed using a significance level of p = 0.05. The critical threshold associated with the p-value was determined as per the formula (Cohen, 2014; Zar, 1999) :

$$ITPC_{crit} = \sqrt{-log(p) * n^{-1}} \qquad (9)$$

where n represents the total count of trials. ITPC values surpassing this threshold were regarded as statistically significant.

4.8.2. Time frequency estimation

In delve deeper into understanding the generation of HERs, we examined the power distribution of HERs time series time-locked to R peaks and shuffled HERs time locked to random peaks. The time-frequency analysis was performed by utilizing wavelet transformation with the *ft_freqanalysis* function from fieldtrip toolbox in MATLAB (Oostenveld et al., 2010). Furthermore, we employed cluster permutation test to find the significant clusters from the time frequency analysis obtained from two conditions i.e., time locked to R peak and activity locked to shuffled R peak using custom built MATLAB code. 1000 iterations of trial randomization were carried out to generate the permutation distribution at every frequency. A two tailed test with a threshold of 0.05 was used to evaluate the time points that exhibit a significant difference in power.

In section 2.8, all the analysis was performed for the 4 to 20 Hz frequency range. This was motivated by earlier findings (Kern et al., 2013) reporting the presence of pulsating artifacts in frequencies below 4 Hz, often attributed to pulsating blood vessels. We restrict our analysis to the 4-20 Hz frequency range to avoid potential artifacts.

4.9. Source localization of HERs

Source localization was performed to obtain the generators of HERs in the brain averaged across all the participants using a current density technique known as exact low-resolution brain electromagnetic tomography (eLORETA), which was implemented using the MATLAB-based fieldtrip toolbox (Oostenveld et al., 2010). The origin (0,0,0) of the colin27 (Holmes et al., 1998) atlas was set to the anterior commissure and fiducials were set accordingly before generating the head model. Using the single shell method (commonly used for MEG), the brain was segmented into a mesh/grid and employing channel position, the leadfield matrix was computed using *ft_prepare_leadfield.* The regularization parameter (l) was set at 0.1 for the localization of brain sources of HERs. Source power at grid locations (32480 grid points) was calculated using *ft_sourceanalysis* on the HERs time series occurring 180-320 ms post R peak for each age group. The HERs activity was normalized against the baseline activity between interval ([-200 -60]) time locked to R peak of the ECG waveform. The source power was then thresholded to the 95th percentile, and the source power that crossed this threshold was considered a significant source of activation. These significant sources were visualized using the *ft_sourceplot* function within Fieldtrip.

4.10. Source time series reconstruction

We reconstructed the time series originating from these significant brain sources participant wise. This was achieved by multiplying the spatial filter generated from the statistically significant grid points for all the 620 participants to the pre-processed HERs time series (channel x time x trials). A consistent headmodel and electrode placement was used across all the participants. Applying the filter to the HERs epoched time seriaes generated three source dipole time series, oriented along the x, y and z axes. Due to the complexity introduced by three dipole orientations, the time series were projected onto the direction of the strongest dipole. This projection was determined by identifying the dominant eigenvector using singular value decomposition (SVD). Further, to simplify the analysis to estimate GC among few nodes, we applied a k-means clustering approach to classify significant grid points into significant clusters. Sources were grouped into 3 clusters. The centroid of each cluster was identified as a brain area using its proximity to the brain anatomical landmark following the MNI atlas. The time series reconstructed trial-wise for each node was the temporal coefficient projected on the first principal component of the dipolar time series obtained from the cluster. The reconstructed time series from each participant was treated as a trial, making a total of 177 trials for the young, 198 trials for the middle and 245 trials for the older age group.

4.11. Granger Causality

We investigated the statistical dependencies among the time series obtained at the source level by computing the directional interaction among the brain nodes of HERs and cardiac signals to understand the age associated changes that can shed light on the compensatory mechanisms. In this pursuit, we employed multivariate Granger Causality (MVGC) analysis to elucidate the direction and magnitude of the causal influence (Dhamala et al., 2008; Granger, 1969) among corticocortical and cortico-cardiac interactions. In its most basic form, we can say that one process, X, Granger causes another process, Y, when X's historical occurrences contribute to forecasting Y's current to a greater extent than what can be achieved by solely considering Y's past events. We conducted the GC analysis using the multivariate granger causality (MVGC) toolbox developed by (Barnett & Seth, 2014). Our dataset consisted of two distinct time series: the neural signal (3 brain nodes) and ECG time series (average taken across all the epochs) for each participant. To meet the prerequisites of the GC algorithm, we assessed the stationarity of these time series using the Augmented Dickey-Fuller test, employing the *'adftest'* function in MATLAB. Since our initial analysis revealed non-stationarity in the time series, we applied a difference transformation to induce stationarity, using MATLAB's *diff* (first order) function. We utilized the vector autoregressive (VAR) model with a lag order of 'p', which was estimated using Akaike Information Criteria (AIC) using the function '*tsdata_to_infocrit*' in MATLAB using the MVGC toolbox (https://in.mathworks.com/matlabcentral/fileexchange/78727-the-multivariate-granger-causality-mvgc-toolbox). We tested various values of VAR order, p = 1, 2, ……, 20. Based on the A/BIC criteria, a VAR order of 3 was chosen for GC estimation. The VAR model is considered robust for the given lag order 'p' when the Akaike Information Criterion (AIC) and Bayesian Information Criterion (BIC) attain their minimum values. This model can be described as (Barnett & Seth, 2014):

$$U_t = \left(\frac{X_t}{Y_t}\right) \qquad (2)$$

where U_t consists of X_t, Y_t as the multivariate processes. The VAR(p) decomposes as

$$\left(\frac{X_t}{Y_t}\right) = \sum_{k=1}^{p} \begin{pmatrix} A_{xx,k} & A_{xy,k} \\ A_{yx,k} & A_{yy,k} \end{pmatrix} \left(\frac{X_{t-k}}{Y_{t-k}}\right) + \left(\frac{\varepsilon_{x,t}}{\varepsilon_{y,t}}\right) \qquad (3)$$

where $A_{xx,k}, A_{xy,k}, A_{yx,k}, A_{yy,k}$ are the regression coefficient and $\varepsilon_{x,t}, \varepsilon_{y,t}$are the residuals and the residuals covariance matrix as

$$\Sigma = cov\begin{pmatrix}\frac{\varepsilon_{x,t}}{\varepsilon_{y,t}}\end{pmatrix} = \begin{pmatrix}\Sigma_{xx} & \Sigma_{xy} \\ \Sigma_{yx} & \Sigma_{yy}\end{pmatrix} \qquad (4)$$

The concept of Granger causality states that if process Y is said to granger cause another process X, when the past instances of Y significantly improve the ability to predict the present values of X compared to solely on X's past events. From this knowledge, two models i.e., reduced regression and full regression model can be generated and demonstrated as:

Full regression model

$$X_t = \sum_{k=1}^{p} A_{xx} \cdot X_{t-k} + \sum_{k=1}^{p} A_{xy} \cdot Y_{t-k} + \varepsilon_{x,t} \qquad (5)$$

Reduced regression model

$$X_t = \sum_{k=1}^{p} A'_{xx} \cdot X_{t-k} + \varepsilon'_{x,t} \qquad (6)$$

Thus, the Granger causality from Y to X is calculated by taking the log-likelihood ratio of the covariance residuals obtained from the full and reduced regression model. Mathematically, Granger causality is depicted as:

$$GC_{Y \rightarrow X} \equiv ln\Sigma'_{xx} \vee \frac{\square}{\Sigma_{xx} \vee} \qquad (7)$$

The significance of the GC values was tested using Geweke's chi squared test using *mvgc_pval* and *significance* function in MVGC toolbox at an alpha value of 0.05.

4.12. Statistical Analysis

4.12.1. Effect of age and gender on HERs

To assess the impact of age on HERs, the time series was divided into three segments based on previous literature (Kamp et al., 2021) : an early phase (180-320 ms post R peak), a middle phase (460-550 ms post R peak), and a late phase (650-750 ms post R peak). We used the *anovan* function in MATLAB for this analysis. We observed a statistically significant difference between the age groups in the early phase window as compared to the middle and late phase time windows. Furthermore, we examined the impact of gender along with age on HERs. As a result, the early phase HERs window i.e., 180-320 ms post R peak, was selected for further analysis. Refer to **Supplementary Table 3** for details.

2.12.2 Eliminating the confound of cardiac field artifact (CFA)

Given that the selected time window for HERs analysis encompasses the period of 180-320 ms after the R peak, which may be susceptible to contamination by cardiac field artifacts, we took measures to address this confounding factor. To mitigate the influence of the cardiac field artifact, we extracted the ECG amplitude specifically within the time window of 180-320 ms following the R peak for each of the 620 participants. Subsequently, we performed a linear regression analysis between the mean ECG amplitude obtained from the 180-320 ms post R peak interval and the HERs obtained from the same interval. This regression analysis aimed to account for the ECG activity as a covariate, effectively eliminating its potential confounding effects on the HERs measurements within the specified time window **(Supplementary Table 5)**.

4.12.3. Linear Regression

Linear regression analysis was performed separately for various parameters (magnitude obtained from peak-to-peak subtraction of HERs in the time interval of 180 to 320ms post R peak, all the cardiovascular measures, estimated ITPC values, GC estimates) as the dependent variable while keeping age as the independent variable.

$$y = \beta_0 + \beta_1 * Age \qquad (8)$$

We utilized *fitlm.m* function within MATLAB to perform a linear regression analysis which yielded F-statistics, regression coefficients and goodness of fit R^2 **(Supplementary 2,4,5)**. To assess the strength of the relationship between variables, we calculated the correlation coefficient using the built-in *corrcoef* function available in MATLAB.

Acknowledgement:

We acknowledge the generous support of NBRC Core funds and computing facility. This study was supported by NBRC Flagship program BT/MEDIII/NBRC/Flagship/Program/2019: Comparative mapping of common mental disorders (CMD) over lifespan. Data collection and sharing for this project was provided by the Cambridge Centre for Ageing and Neuroscience (Cam-CAN). Cam-CAN funding was provided by the UK Biotechnology and Biological Sciences Research council (grant number BB/H008217/1), together with support from the UK Medical Research Council and University of Cambridge, UK. In accordance with the data usage agreement for Cam-CAN dataset, the article has been submitted as open access.

Conflict of Interest Statement

All authors declare no conflict of interest scenario exist.

Author Credits

Kirti Saluja: Conceptualization, Formal analysis, methods, Validation, Visualization, Writing-Original draft preparation and editing.

Dipanjan Roy: Supervision, Writing-Reviewing and editing.

Arpan Banerjee: Conceptualization, Resources, Visualization, Writing-Reviewing and editing, Funding acquisition, Supervision.

References:

Al, E., Iliopoulos, F., Forschack, N., Nierhaus, T., Grund, M., Motyka, P., Gaebler, M., Nikulin, V. V., & Villringer, A. (2020). Heart–brain interactions shape somatosensory perception and evoked potentials. *Proceedings of the National Academy of Sciences*, *117*(19), 10575–10584. https://doi.org/10.1073/pnas.1915629117

Azzalini, D., Rebollo, I., & Tallon-Baudry, C. (2019). Visceral Signals Shape Brain Dynamics and Cognition. *Trends in Cognitive Sciences*, *23*(6), 488–509. https://doi.org/10.1016/j.tics.2019.03.007

Babo-Rebelo, M., Wolpert, N., Adam, C., Hasboun, D., & Tallon-Baudry, C. (2016). Is the cardiac monitoring function related to the self in both the default network and right anterior insula? *Philosophical Transactions of the Royal Society B: Biological Sciences*, *371*(1708), 20160004. https://doi.org/10.1098/rstb.2016.0004

Banellis, L., & Cruse, D. (2020). Skipping a Beat: Heartbeat-Evoked Potentials Reflect Predictions during Interoceptive-Exteroceptive Integration. *Cerebral Cortex Communications*, *1*(1), tgaa060. https://doi.org/10.1093/texcom/tgaa060

Barnett, L., & Seth, A. K. (2014). The MVGC multivariate Granger causality toolbox: A new approach to Granger-causal inference. *Journal of Neuroscience Methods*, *223*, 50–68. https://doi.org/10.1016/j.jneumeth.2013.10.018

Cabeza, R., & Dennis, N. A. (2013). *Frontal lobes and aging: Deterioration and Compensation*.

Chen, Z., Venkat, P., Seyfried, D., Chopp, M., Yan, T., & Chen, J. (2017). Brain–Heart Interaction. *Circulation Research, 121*(4), 451–468. https://doi.org/10.1161/CIRCRESAHA.117.311170

Climie, R. E., Alastruey, J., Mayer, C. C., Schwarz, A., Laucyte-Cibulskiene, A., Voicehovska, J., Bianchini, E., Bruno, R.-M., Charlton, P. H., Grillo, A., Guala, A., Hallab, M., Hametner, B., Jankowski, P., Königstein, K., Lebedeva, A., Mozos, I., Pucci, G., Puzantian, H., … on behalf of the VascAgeNet Education and Dissemination Working Group. (2023). Vascular ageing: Moving from bench towards bedside. *European Journal of Preventive Cardiology, 30*(11), 1101–1117. https://doi.org/10.1093/eurjpc/zwad028

Cohen, M. X. (2014). *Analyzing Neural Time Series Data: Theory and Practice*. MIT Press.

Craig, A. D. (2002). How do you feel? Interoception: the sense of the physiological condition of the body. *Nature Reviews Neuroscience*, *3*(8), Article 8. https://doi.org/10.1038/nrn894

Critchley, H. D., Wiens, S., Rotshtein, P., Ohman, A., & Dolan, R. J. (2004). Neural systems supporting interoceptive awareness. *Nature Neuroscience*, *7*(2), 189–195. https://doi.org/10.1038/nn1176

de Dieuleveult, A. L., Siemonsma, P. C., van Erp, J. B. F., & Brouwer, A.-M. (2017). Effects of Aging in Multisensory Integration: A Systematic Review. *Frontiers in Aging Neuroscience*, *9*. https://doi.org/10.3389/fnagi.2017.00080

Dhamala, M., Rangarajan, G., & Ding, M. (2008). Analyzing information flow in brain networks with nonparametric Granger causality. *NeuroImage, 41*(2), 354–362. https://doi.org/10.1016/j.neuroimage.2008.02.020

Eckberg, D. L., & Sleight, P. (1992). *Human Baroreflexes in Health and Disease*. Oxford University Press. https://doi.org/10.1093/oso/9780198576938.001.0001

Garfinkel, S. N., Minati, L., Gray, M. A., Seth, A. K., Dolan, R. J., & Critchley, H. D. (2014). Fear from the Heart: Sensitivity to Fear Stimuli Depends on Individual Heartbeats. *The Journal of Neuroscience*, *34*(19), 6573–6582. https://doi.org/10.1523/JNEUROSCI.3507-13.2014

Garfinkel, S. N., Seth, A. K., Barrett, A. B., Suzuki, K., & Critchley, H. D. (2015). Knowing your own heart: Distinguishing interoceptive accuracy from interoceptive awareness. *Biological Psychology, 104*, 65–74. https://doi.org/10.1016/j.biopsycho.2014.11.004

Gauthier, C. J., Madjar, C., Desjardins-Crépeau, L., Bellec, P., Bherer, L., & Hoge, R. D. (2013). Age dependence of hemodynamic response characteristics in human functional magnetic resonance imaging. *Neurobiology of Aging, 34*(5), 1469–1485. https://doi.org/10.1016/j.neurobiolaging.2012.11.002

Geweke, J. (1982). Measurement of Linear Dependence and Feedback between Multiple Time Series. *Journal of the American Statistical Association*. https://www.tandfonline.com/doi/abs/10.1080/01621459.1982.10477803

Granger, C. W. J. (1969). Investigating Causal Relations by Econometric Models and Cross-spectral Methods. *Econometrica, 37*(3), 424–438. https://doi.org/10.2307/1912791

Gray, M. A., Taggart, P., Sutton, P. M., Groves, D., Holdright, D. R., Bradbury, D., Brull, D., & Critchley, H. D. (2007). A cortical potential reflecting cardiac function. *Proceedings of the National Academy of Sciences of the United States of America*, *104*(16), 6818–6823. https://doi.org/10.1073/pnas.0609509104

Jayakody, D. M. P., Friedland, P. L., Martins, R. N., & Sohrabi, H. R. (2018). Impact of Aging on the Auditory System and Related Cognitive Functions: A Narrative Review. *Frontiers in Neuroscience, 12*. https://doi.org/10.3389/fnins.2018.00125

Kallmünzer, B., Breuer, L., Kahl, N., Bobinger, T., Raaz-Schrauder, D., Huttner, H. B., Schwab, S., & Köhrmann, M. (2012). Serious Cardiac Arrhythmias After Stroke. *Stroke, 43*(11), 2892–2897. https://doi.org/10.1161/STROKEAHA.112.664318

Kamiński, M., Ding, M., Truccolo, W. A., & Bressler, S. L. (2001). Evaluating causal relations in neural systems: Granger causality, directed transfer function and statistical assessment of significance. *Biological Cybernetics*, *85*(2), 145–157. https://doi.org/10.1007/s004220000235

Kamp, S.-M., Schulz, A., Forester, G., & Domes, G. (2021). Older adults show a higher heartbeat-evoked potential than young adults and a negative association with everyday metacognition. *Brain Research*, *1752*, 147238. https://doi.org/10.1016/j.brainres.2020.147238

Kang, W., Wang, J., & Malvaso, A. (2022). Inhibitory Control in Aging: The Compensation-Related Utilization of Neural Circuits Hypothesis. *Frontiers in Aging Neuroscience, 13*, 771885. https://doi.org/10.3389/fnagi.2021.771885

Kern, M., Aertsen, A., Schulze-Bonhage, A., & Ball, T. (2013). Heart cycle-related effects on event-related potentials, spectral power changes, and connectivity patterns in the human ECoG. *NeuroImage*, *81*, 178–190. https://doi.org/10.1016/j.neuroimage.2013.05.042

Khalsa, Rudrauf, D., & Tranel, D. (2009). Interoceptive awareness declines with age. *Psychophysiology*, *46*(6), 1130–1136. https://doi.org/10.1111/j.1469-8986.2009.00859.x

Khalsa, S. S., & Verdonk, C. (2022). Atrial Fibrillation as a Disorder of Heart-Brain Communication∗. *JACC: Clinical Electrophysiology*, *8*(10), 1231–1233. https://doi.org/10.1016/j.jacep.2022.07.021

Kim, J., & Jeong, B. (2019). Heartbeat Induces a Cortical Theta-Synchronized Network in the Resting State. *eNeuro*, *6*(4), ENEURO.0200-19.2019. https://doi.org/10.1523/ENEURO.0200-19.2019

Krishnamoorthy, V., Mackensen, G. B., Gibbons, E. F., & Vavilala, M. S. (2016). Cardiac Dysfunction After Neurologic Injury: What Do We Know and Where Are We Going? *CHEST*, *149*(5), 1325–1331. https://doi.org/10.1016/j.chest.2015.12.014

Kumral, D., Al, E., Cesnaite, E., Kornej, J., Sander, C., Hensch, T., Zeynalova, S., Tautenhahn, S., Hagendorf, A., Laufs, U., Wachter, R., Nikulin, V., & Villringer, A. (2022). Attenuation of the Heartbeat-Evoked Potential in Patients With Atrial Fibrillation. *JACC: Clinical Electrophysiology*, *8*(10), 1219–1230. https://doi.org/10.1016/j.jacep.2022.06.019

Luft, C. D. B., & Bhattacharya, J. (2015). Aroused with heart: Modulation of heartbeat evoked potential by arousal induction and its oscillatory correlates. *Scientific Reports*, *5*(1), Article 1. https://doi.org/10.1038/srep15717

Montoya, P., Schandry, R., & Müller, A. (1993). Heartbeat evoked potentials (HEP): Topography and influence of cardiac awareness and focus of attention. *Electroencephalography and Clinical Neurophysiology/Evoked Potentials Section*, *88*(3), 163–172. https://doi.org/10.1016/0168-5597(93)90001-6

Murphy, J., Geary, H., Millgate, E., Catmur, C., & Bird, G. (2018). Direct and indirect effects of age on interoceptive accuracy and awareness across the adult lifespan. *Psychonomic Bulletin & Review*, *25*(3), 1193–1202. https://doi.org/10.3758/s13423-017-1339-z

North, B. J., & Sinclair, D. A. (2012). The Intersection Between Aging and Cardiovascular Disease. *Circulation Research*, *110*(8), 1097–1108. https://doi.org/10.1161/CIRCRESAHA.111.246876

Oostenveld, R., Fries, P., Maris, E., & Schoffelen, J.-M. (2010). FieldTrip: Open Source Software for Advanced Analysis of MEG, EEG, and Invasive Electrophysiological Data. *Computational Intelligence and Neuroscience*, *2011*, e156869. https://doi.org/10.1155/2011/156869

Padeiro, M., Santana, P., & Grant, M. (2023). Chapter 1—Global aging and health determinants in a changing world. In P. J. Oliveira & J. O. Malva (Eds.), *Aging* (pp. 3–30). Academic Press. https://doi.org/10.1016/B978-0-12-823761-8.00021-5

Park, H.-D., Bernasconi, F., Salomon, R., Tallon-Baudry, C., Spinelli, L., Seeck, M., Schaller, K., & Blanke, O. (2018). Neural Sources and Underlying Mechanisms of Neural Responses to Heartbeats, and their Role in Bodily Self-consciousness: An Intracranial EEG Study. *Cerebral Cortex*, *28*(7), 2351–2364. https://doi.org/10.1093/cercor/bhx136

Park, H.-D., Correia, S., Ducorps, A., & Tallon-Baudry, C. (2014). Spontaneous fluctuations in neural responses to heartbeats predict visual detection. *Nature Neuroscience*, *17*(4), Article 4. https://doi.org/10.1038/nn.3671

Pathak, A., Sharma, V., Roy, D., & Banerjee, A. (2022). Biophysical mechanism underlying compensatory preservation of neural synchrony over the adult lifespan. *Communications Biology*, *5*(1), Article 1. https://doi.org/10.1038/s42003-022-03489-4

Peters, R. (2006). Ageing and the brain. *Postgraduate Medical Journal*, *82*(964), 84–88. https://doi.org/10.1136/pgmj.2005.036665

Petzschner, F. H., Weber, L. A., Wellstein, K. V., Paolini, G., Do, C. T., & Stephan, K. E. (2019). Focus of attention modulates the heartbeat evoked potential. *NeuroImage*, *186*, 595–606. https://doi.org/10.1016/j.neuroimage.2018.11.037

Pollatos, O., & Schandry, R. (2004). Accuracy of heartbeat perception is reflected in the amplitude of the heartbeat-evoked brain potential. *Psychophysiology*, *41*(3), 476–482. https://doi.org/10.1111/1469-8986.2004.00170.x

Rauschecker, J. P., & Tian, B. (2000). Mechanisms and streams for processing of “what” and “where” in auditory cortex. *Proceedings of the National Academy of Sciences of the United States of America*, *97*(22), 11800–11806. https://doi.org/10.1073/pnas.97.22.11800

Sahoo, B., Pathak, A., Deco, G., Banerjee, A., & Roy, D. (2020). Lifespan associated global patterns of coherent neural communication. *NeuroImage*, *216*, 116824. https://doi.org/10.1016/j.neuroimage.2020.116824

Saunders, B. A., & Jenkins, L. C. (1973). Cardiac arrhythmias of central nervous system origin: Possible mechanism and suppression. *Canadian Anaesthetists’ Society Journal*, *20*(5), 617–628. https://doi.org/10.1007/BF03026259

Schulz, A., Köster, S., Beutel, M. E., Schächinger, H., Vögele, C., Rost, S., Rauh, M., & Michal, M. (2015). Altered Patterns of Heartbeat-Evoked Potentials in Depersonalization/Derealization Disorder: Neurophysiological Evidence for Impaired Cortical Representation of Bodily Signals. *Psychosomatic Medicine*, *77*(5), 506. https://doi.org/10.1097/PSY.0000000000000195

Shafto, M. A., Tyler, L. K., Dixon, M., Taylor, J. R., Rowe, J. B., Cusack, R., Calder, A. J., Marslen-Wilson, W. D., Duncan, J., Dalgleish, T., Henson, R. N., Brayne, C., Matthews, F. E., & Cam-CAN. (2014). The Cambridge Centre for Ageing and Neuroscience (Cam-CAN) study protocol: A cross-sectional, lifespan, multidisciplinary examination of healthy cognitive ageing. *BMC Neurology*, *14*(1), 204. https://doi.org/10.1186/s12883-014-0204-1

Shen, M. J., & Zipes, D. P. (2014). Role of the Autonomic Nervous System in Modulating Cardiac Arrhythmias. *Circulation Research*, *114*(6), 1004–1021. https://doi.org/10.1161/CIRCRESAHA.113.302549

Spreng, R. N., & Turner, G. R. (2019). The Shifting Architecture of Cognition and Brain Function in Older Adulthood. *Perspectives on Psychological Science: A Journal of the Association for Psychological Science*, *14*(4), 523–542. https://doi.org/10.1177/1745691619827511

Taylor, J. R., Williams, N., Cusack, R., Auer, T., Shafto, M. A., Dixon, M., Tyler, L. K., Cam-CAN, & Henson, R. N. (2017). The Cambridge Centre for Ageing and Neuroscience (Cam-CAN) data repository: Structural and functional MRI, MEG, and cognitive data from a cross-sectional adult lifespan sample. *Neuroimage*, *144*(Pt B), 262. https://doi.org/10.1016/j.neuroimage.2015.09.018

Terhaar, J., Viola, F. C., Bär, K.-J., & Debener, S. (2012). Heartbeat evoked potentials mirror altered body perception in depressed patients. *Clinical Neurophysiology*, *123*(10), 1950–1957. https://doi.org/10.1016/j.clinph.2012.02.086

Thayer, J. F., & Lane, R. D. (2000). A model of neurovisceral integration in emotion regulation and dysregulation. *Journal of Affective Disorders*, *61*(3), 201–216. https://doi.org/10.1016/S0165-0327(00)00338-4

Thayer, J. F., & Lane, R. D. (2009). Claude Bernard and the heart–brain connection: Further elaboration of a model of neurovisceral integration. *Neuroscience & Biobehavioral Reviews*, *33*(2), 81–88. https://doi.org/10.1016/j.neubiorev.2008.08.004

Thuwal, K., Banerjee, A., & Roy, D. (2021). Aperiodic and Periodic Components of Ongoing Oscillatory Brain Dynamics Link Distinct Functional Aspects of Cognition across Adult Lifespan. *eNeuro*, *8*(5), ENEURO.0224-21.2021. https://doi.org/10.1523/ENEURO.0224-21.2021

Van Diepen, R. M., & Mazaheri, A. (2018). The Caveats of observing Inter-Trial Phase-Coherence in Cognitive Neuroscience. *Scientific Reports*, *8*(1), 2990. https://doi.org/10.1038/s41598-018-20423-z

Zanto, T. P., & Gazzaley, A. (2019). Aging of the frontal lobe. *Handbook of Clinical Neurology*, *163*, 369–389. https://doi.org/10.1016/B978-0-12-804281-6.00020-3

Zar, J. H. (1999). *Biostatistical Analysis*. Pearson Education India.

Figure Captions

Figure 1: Overview of the Data Preprocessing and Analysis Pipeline

Simultaneous MEG-ECG recordings undergo a preprocessing pipeline including detrending, bandpass filtering and artifact removal using Independent Component Analysis (ICA). R peaks are detected from the electrocardiogram (ECG) waveform using the Pan-Tompkin algorithm, serving as a trigger point to compute heartbeat evoked responses (HERs). HERs are computed across all the age-groups (young, middle and old). Additionally, wavelet analysis is employed to investigate the mechanisms underlying HERs generation. Source localization using eLORETA identifies cortical sources underlying HERs. Finally, Granger Causality maps causal functional relationships among cortical sources of HERs.

Figure 2: Cardiovascular measures across age

(A) Methods used to capture cardiac activity includes electrocardiogram (ECG) and sphygmomanometer which measures cardiovascular activities such as electric activity of the cardiac muscles and blood pressure respectively. Cardiovascular parameters include: Interbeat interval (IBI), Heart rate variability (HRV), Heart Rate (HR), Systolic and Diastolic blood pressure (B) IBI significantly decreases ($r= - 0.0994$; $p = 0.0133$) (C) HRV does not change ($r = -0.0022$; $p =0.9573$) (D) HR significantly increases ($r = 0.1121$; $p= 0.0052$) (E) Systolic blood pressure significantly increases ($r = 0.4370$; $p<0.001$) and (F) Diastolic blood pressure remains unchanged ($r = 0.0734$; $p = 0.0910$) across age

Figure 3: Heartbeat evoked responses (HERs) across age and gender

(A) Method: Simultaneous MEG-ECG recording; using R peak of the ECG waveform as the time points to epoch neural time series to obtain the HERs (B) Group wise analysis of HERs obtained from time locked MEG activity to R peak of the ECG waveform. Statistical test conducted indicates that the HERs differences across age groups are significant shown by the asterisks ($F(2,619) = 9.48$; $p<0.001$). (C) Group wise analysis of HERs obtained from time locked activity to the shuffle ECG time series (sanity check) (D) Linear regression conducted between magnitude (obtained from peak to peak subtraction) of HERs and age ($r= -0.1963$; $p<0.001$) (E) shows the group-wise analysis of HERs i.e., time locked MEG activity to the R peak (represented by the dotted line) of the ECG waveform for two genders (male and female). Statistical test conducted indicates that there is no significant difference between the two groups $f(1,619) = 0.02$; $P = 0.8801$). The shaded area shows the standard deviation. Linear regression conducted between magnitude (obtained from peak to peak subtraction) of HERs across age in F) Females ($r= -0.2161$; $P<0.001$) and (G) Males ($r = -0.1735$; $p<0.01$)

Figure 4: Mechanism of Heartbeat Evoked Responses

Inter trial phase coherence (ITPC) was computed on evoked data time locked to (A) R peak and (B) shuffled R peak of ECG waveform calculated across all the age groups. ITPC values within the white boundary are considered to be statistically significant, using critical value at $p = 0.05$. Time frequency spectrograms calculated on evoked data time locked to (C) R peak and (D) shuffled R peak of ECG waveform (found no significant difference between the age groups; cluster permutation test at $p =0.05$) () (E) ITPC value (extracted from each subject) in theta band significantly increases across age ($r= 0.2236$; $p< 0.001$). (F) No correlation observed between mean ITPC values and mean power extracted at around 180-320 ms post R peak of the ECG waveform for each participant (r = 0.0596; p = 0.1382).

Figure 5: Cortical sources of Heartbeat Evoked Responses (HERs)

The sources represent the cortical sources involved in the processing of heartbeat which includes right anterior prefrontal cortex, right orbitofrontal cortex and left temporal pole. The statistical threshold was set at 95th percentile and the source powers of grid points to surpassing this threshold were considered as significant sources of activation. All regions were approximated to the nearest Broadmann areas of the human brain. R represents right and L represents left hemisphere of the brain

Figure 6: Directed interactions among cortico-cortical nodes across age

To investigate the directional interaction among the cortical sources involved in the processing of cardiac information, we computed Granger causality (GC). (A) Heatmaps depicting pairwise GC values among HERs sources. The significance of the GC values was tested using Geweke's chi squared test at alpha value of 0.05. All the significant GC values were marked with white boxes. (B) Schematic illustration of directed connectivity among the HERs sources demonstrating a bidirectional connectivity between L Temporal Pole and R Orbitofrontal cortex, R Anterior Prefrontal Cortex and R Orbitofrontal Cortex and unidirectional connectivity between R Anterior Prefrontal Cortex to L TemporalePole. Linear regression conducted between the GC values obtained from each directed interaction across age. Trend of GC values (C) from R Orbitofrontal Cortex to R Anterior Prefrontal Cortex (r= -0.0742) (D) R Orbitofrontal Cortex to L Temporal Pole (r = 0.0593) remained unchanged (E) L Temporal Pole to R Orbitofronal Cortex significantly increases (r = 0.1728***) (F) R Anterior Prefrontal

Cortex to LTemporal Pole significantly increases (r = 0.1530***) (G) R Anterior Prefrontal Cortex to R Orbitofronal Cortex remained increases (r = 0.0990*) across age.

Resting state MEG signal

Preprocessing:
Head motion correction, Detrended, Bandpass filtered 1-45 Hz, ICA correction

Resting state ECG signal

Preprocessing:
Quality check using statistical parameters, Detrended, Locating R peaks using Pan-Tompkin algorithm

Heartbeat evoked responses (HERs)

Foundation of HERs generation

Inter-trial phase coherence

Time frequency analysis

Source localisation

Forward Model

Inverse Model

Representation of the brain activity on the cortical surface

Granger Causality

To understand the direction and strength of causality between the brain nodes obtained from source localisation

$\times 10^{-14}$
***
1
0
-1
Amplitude (fT)
-200
0
200
400
600
800
Time (ms)
20
15
10
5
0
200
400
600
800
0.1
0.15
0.2
20
15
10
5
0 200 400 600 800
$\times 10^{-24}$
1
2
3
R Ant. PFC
R OFC
L Temp Pole

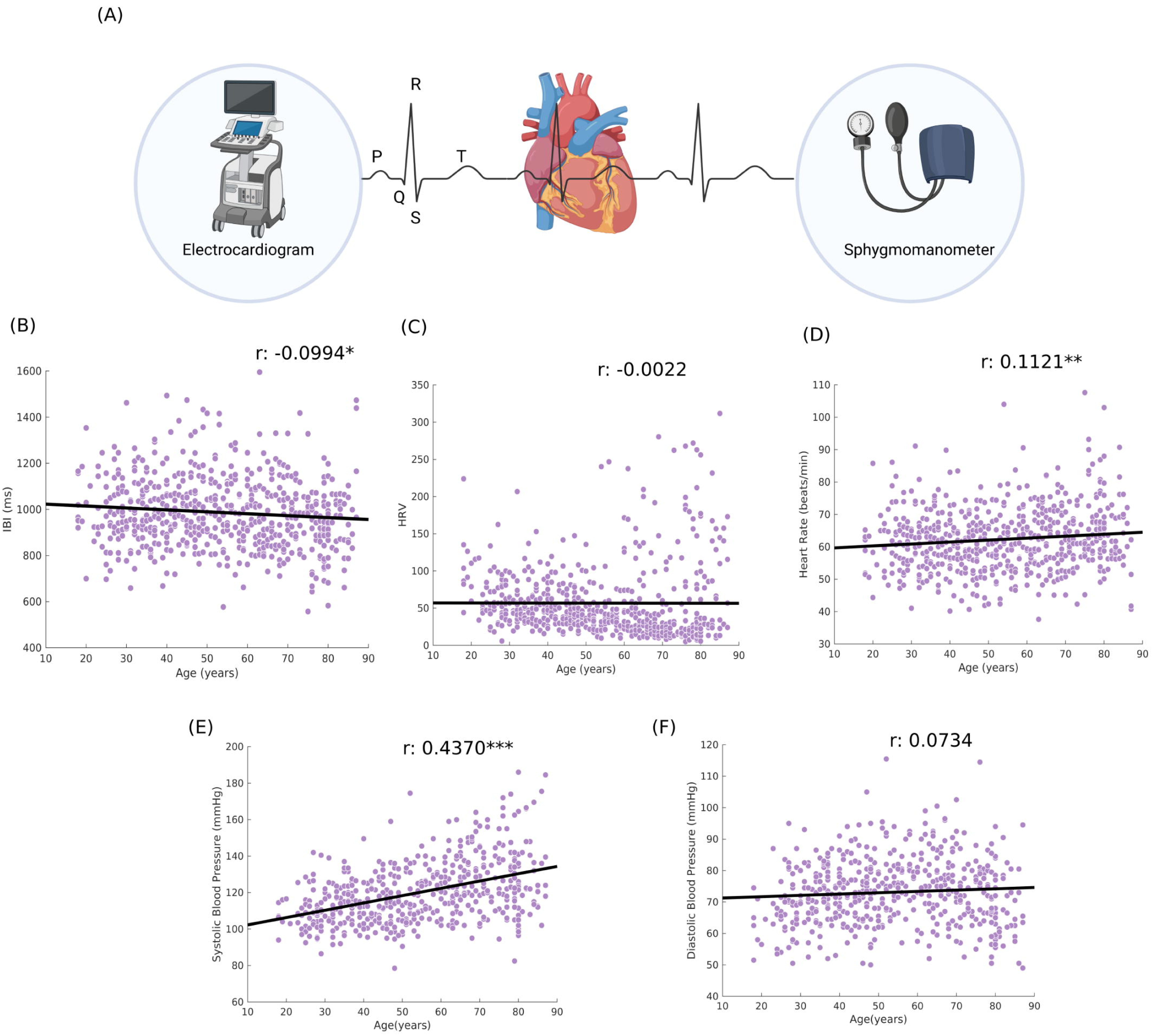
(A)
R
P
T
Q
S
Electrocardiogram
Sphygmomanometer
(B)
r: -0.0994*
IBI (ms)
1600
1400
1200
1000
800
600
400
10
20
30
40
50
60
70
80
90
Age (years)
(C)
r: -0.0022
HRV
350
300
250
200
150
100
50
0
10
20
30
40
50
60
70
80
90
Age (years)
(D)
r: 0.1121**
Heart Rate (beats/min)
110
100
90
80
70
60
50
40
30
10
20
30
40
50
60
70
80
90
Age (years)
(E)
r: 0.4370***
Systolic Blood Pressure (mmHg)
200
180
160
140
120
100
80
60
10
20
30
40
50
60
70
80
90
Age(years)
(F)
r: 0.0734
Diastolic Blood Pressure (mmHg)
120
110
100
90
80
70
60
50
40
10
20
30
40
50
60
70
80
90
Age(years)

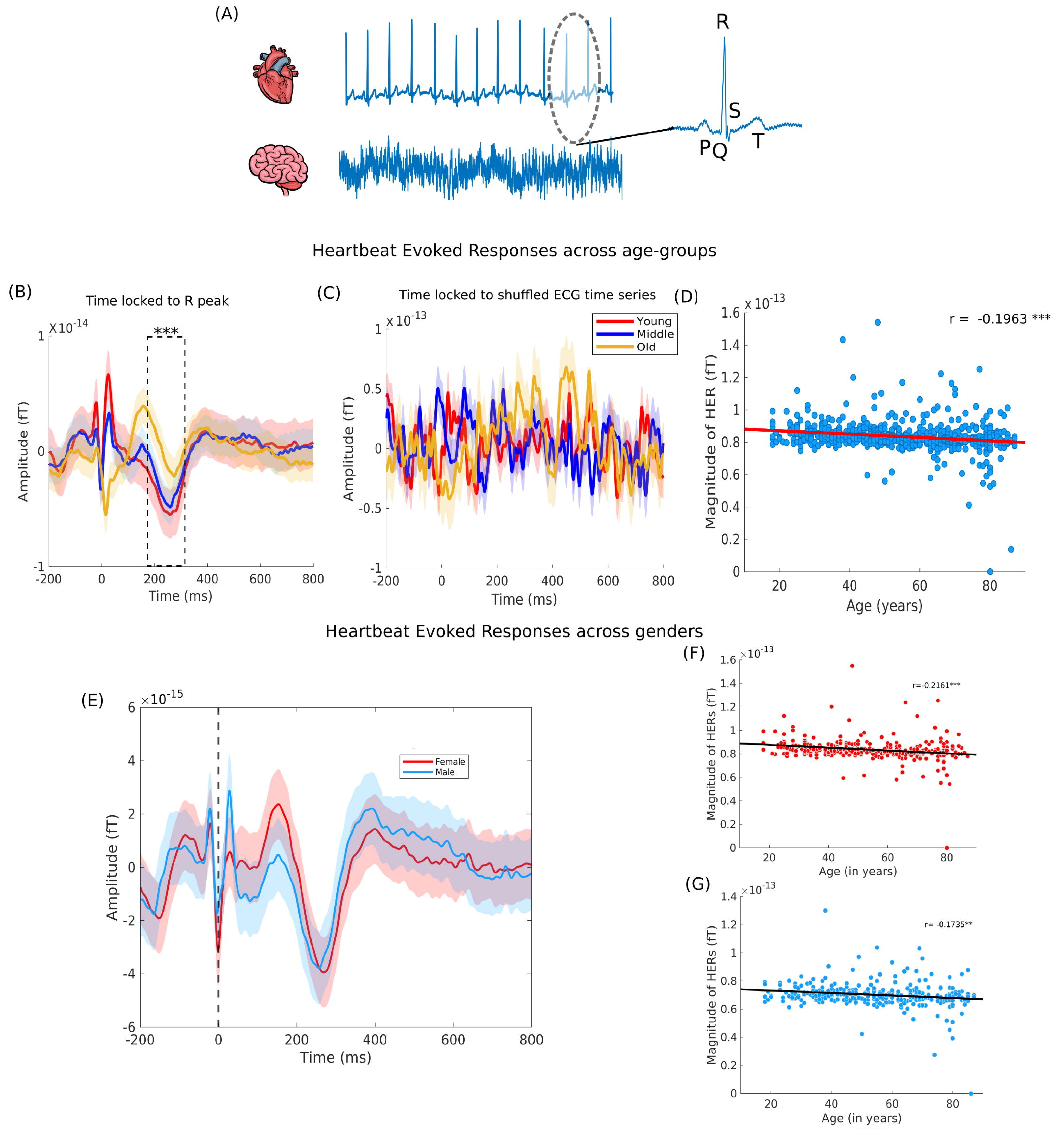
(A)
R
S
PQ
T
Heartbeat Evoked Responses across age-groups
(B)
Time locked to R peak
X10-14
***
Amplitude (fT)
Time (ms)
1
0
-1
-200
0
200
400
600
800
(C)
Time locked to shuffled ECG time series
x 10-13
Young
Middle
Old
Amplitude (fT)
Time (ms)
1
0.5
0
-0.5
-1
(D)
x 10-13
r = -0.1963 ***
Magnitude of HER (fT)
Age (years)
1.6
1.4
1.2
1
0.8
0.6
0.4
0.2
0
20
40
60
80
Heartbeat Evoked Responses across genders
(E)
×10-15
Female
Male
Amplitude (fT)
Time (ms)
6
4
2
0
-2
-4
-6
(F)
×10-13
r=-0.2161***
Magnitude of HERs (fT)
Age (in years)
(G)
×10-13
r= -0.1735**
Magnitude of HERs (fT)
Age (in years)

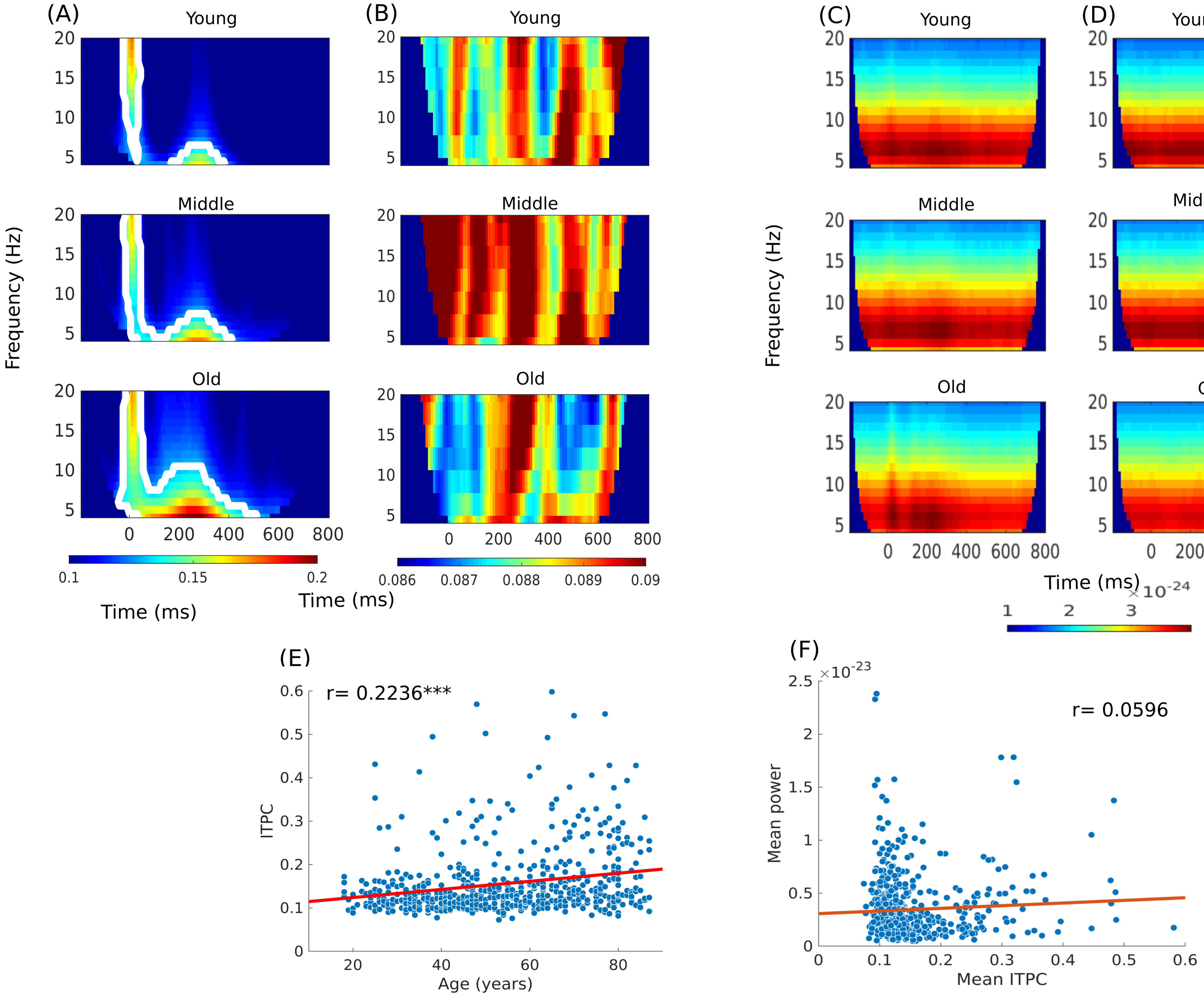
(A)
Young
Middle
Old
Frequency (Hz)
20
15
10
5
0
200
400
600
800
0.1
0.15
0.2
Time (ms)
(B)
Young
Middle
Old
0.086
0.087
0.088
0.089
0.09
Time (ms)
(C)
Young
Middle
Old
Frequency (Hz)
(D)
Young
Middle
Old
Time (ms)
×10-24
1
2
3
(E)
r= 0.2236***
ITPC
0.6
0.5
0.4
0.3
0.2
0.1
0
20
40
60
80
Age (years)
(F)
×10-23
2.5
2
1.5
1
0.5
0
r= 0.0596
Mean power
0
0.1
0.2
0.3
0.4
0.5
0.6
Mean ITPC

L
R

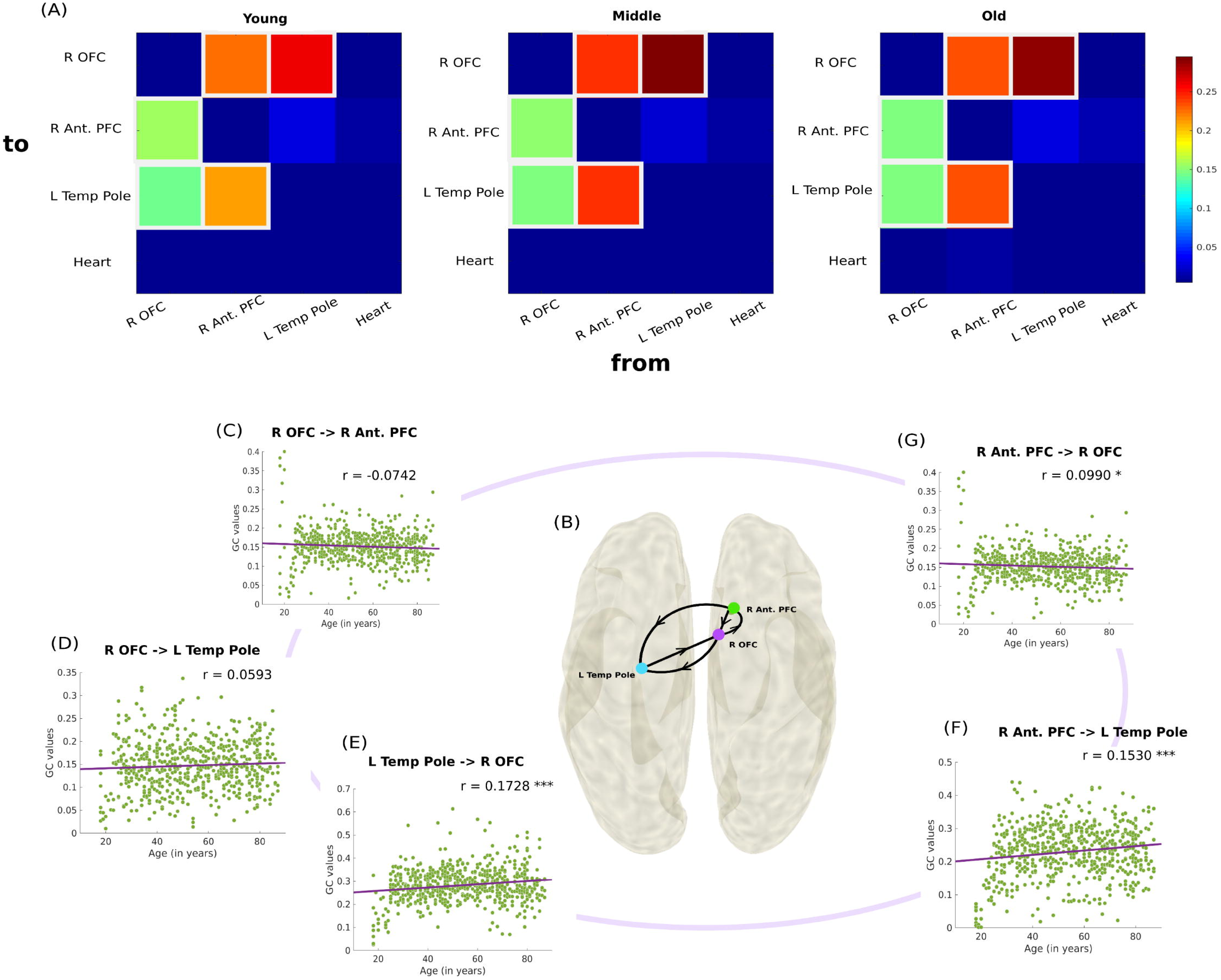

(A)
Young
Middle
Old
to
from
R OFC
R Ant. PFC
L Temp Pole
Heart
0.25
0.2
0.15
0.1
0.05
(B)
R Ant. PFC
R OFC
L Temp Pole
(C)
R OFC -> R Ant. PFC
r = -0.0742
(D)
R OFC -> L Temp Pole
r = 0.0593
(E)
L Temp Pole -> R OFC
r = 0.1728 ***
(F)
R Ant. PFC -> L Temp Pole
r = 0.1530 ***
(G)
R Ant. PFC -> R OFC
r = 0.0990 *
GC values
Age (in years)
20
40
60
80